ELSEVIER

Journal of Fluids and Structures 23 (2007) 227–248

JOURNAL OF FLUIDS AND STRUCTURES

www.elsevier.com/locate/jfs

Transition phenomena in the wake of a square cylinder

S.C. Luo[a,*], X.H. Tong[b], B.C. Khoo[a]

[a]*Department of Mechanical Engineering, 10 Kent Ridge Crescent, National University of Singapore, Singapore 119260, Singapore*
[b]*China Knowledge Consulting, 8 Temasek Boulevard, #37-01A Suntec Tower Three, Singapore 038988, Singapore*

Received 6 July 2005; accepted 12 August 2006
Available online 30 October 2006

Abstract

The transition phenomena in the wake of a square cylinder were investigated. The existence of mode A and mode B instabilities in the wake of a square cylinder was demonstrated. The critical Reynolds numbers for the inception of these instability modes were identified through the determination of discontinuities in the St–Re curves, and were found to have mean values of 160 and 204 for the onset of mode A and B instabilities, respectively. The spectra and time traces of the wake streamwise velocity component were found to display three distinct patterns in laminar, mode A and mode B flow regimes. Streamwise vortices with different wavelength at various Reynolds numbers were observed through different measures. The symmetries and evolution of the secondary vortices were observed using laser-induced-fluorescent dye. It was found that, just like the case of a circular cylinder, the secondary vortices from the top and bottom rows were out-of-phase with each other in the mode A regime, but in-phase with each other in the mode B regime. From the flow visualization, it was qualitatively proven that there is stronger interaction between braid regions in the mode B regime. At the same time, analysis of PIV measurements quantitatively demonstrated the presence of the stronger cross flow in mode B regime when compared to the mode A regime. It suggests that the in-phase symmetry of the mode B instability is the result of strong interaction between the top and bottom vortex rows. It was also observed that although the vorticity of the secondary vortices in the mode A regime was smaller, its circulation was more than twice that of mode B instability. Compared to primary vortices, the circulations of both mode A and mode B vortices were much smaller, which indicates that the secondary vortices most likely originate from the primary vortices. The wavelengths of the streamwise vortices in the mode A and B regimes were measured using the auto-correlation method, and were found to be 5.1 ($\pm$0.1)D, 1.3 ($\pm$0.1)D, and 1.1 ($\pm$0.1)D at Re = 183 (mode A), 228 and 377 (both mode B), respectively. From the present investigation, mode A instability was likely to be due to the joint-effects of the deformation of primary vortex cores and the stretching of vortex sheets in the braid region. On the other hand, mode B instability was thought to originate from the "imprinting" process.

1. Introduction

Square and circular cylinders are very commonly used shapes in engineering. However, when compared with the wake of a circular cylinder which has been extensively studied, the wake of a square cylinder is somewhat less thoroughly investigated, especially experimentally. At the same time, even for the case of a circular cylinder wake, some

*Corresponding author.
E-mail address: mpeluosc@nus.edu.sg (S.C. Luo).

0889-9746/$ - see front matter © 2006 Elsevier Ltd. All rights reserved.
doi:10.1016/j.jfluidstructs.2006.08.012

unresolved problems remain. Therefore, the authors were motivated to (experimentally) study the transition processes in the wake of a square cylinder, and hope to contribute toward a better understanding of the bluff body wake transition process.

From the work by Williamson and other researchers, it was established that the circular cylinder wake transition involves two modes of small-scale three-dimensional instability. They are called modes "A" and "B", and occur in different Reynolds number ranges. Williamson (1988b, 1996a) proposed that the transition to three-dimensionality in the wake of circular cylinder could conveniently be described in reference to two discontinuities in the St–Re (Strouhal number versus Reynolds number) relation curve. At the first discontinuity, the Strouhal number drops from the laminar flow regime curve to one that corresponds to mode A three-dimensional shedding; this discontinuity is hysteretic. As Re is increased, there is a second, less sharp discontinuity (increase) in the Strouhal number, indicating the beginning of the mode B instability regime. This second discontinuity is not hysteretic, and involves a gradual transfer of energy from mode A to mode B as Re increases.

Williamson (1996a, b) pointed out that these two modes are quite distinct in spanwise length scale and spatial symmetry, and were found to scale on different physical features of the flow. Mode A instability has a spanwise wavelength of about three to four cylinder diameters and the top and bottom row secondary vortices are out-of-phase to each other. On the other hand, mode B is characterized by a shorter spanwise wavelength of about one cylinder diameter and exhibits an in-phase pattern between the top and bottom rows. Mode A structure is clearly evident in the range $190 < Re < 240$. At higher Reynolds number, around and above $Re = 240$, mode B is observed. When Re is above 260, only mode B can be detected.

The existence of these two transition modes has been confirmed by other experiments for the case of the circular cylinder wake by Bays-Muchmore and Ahmed (1993) (mode B), Wu et al. (1994, 1996) (mode B) and Brede et al. (1996) (modes A and B).

The three-dimensionality of the circular cylinder wake transition had also been observed in DNS of circular cylinder wake (Karniadakis and Triantafyllou, 1992; Zhang et al., 1995; Mittal, 1994; Mittal and Balachandar, 1995b; Henderson, 1997; Thompson et al., 1994, 1996). All of these investigations confirmed the existence of mode A and mode B instabilities. In addition, Barkley and Henderson (1996) investigated the circular cylinder wake using Floquet stability analysis and obtained comparable results.

Although there is some consensus on the circular cylinder wake transition process, the mechanism of the transition process remains controversial. Suggested causes of mode A instability include elliptic instability of the primary vortex cores (Williamson, 1996a), and centrifugal instability of the braid region between the primary vortices (Brede et al., 1996). On the other hand, it was suggested that mode B instability could be due to hyperbolic instability associated with the braid region connecting adjacent spanwise vortices (Williamson, 1996a), or from the instability of the separated shear layers in the immediate wake of the cylinder (Brede et al., 1996). Other related discussion can be found in Henderson (1997) and more recently in Thompson et al. (2001) and Blackburn and Lopez (2003a).

Besides the circular cylinder, investigation of the three-dimensional vortical structures in the wake of elliptic cylinders was carried out by Mittal and Balachandar (1995a) and for a normal flat plate by Najjar and Balachandar (1996, 1998). Both studies suggested that, at modest Reynolds numbers, there exists an instability mode that is similar to the mode B instability observed in the wake of a circular cylinder.

As for a square cylinder, although there are a number of papers reporting on experimental investigations on flow past a square cylinder in the literature [e.g., Okajima (1982), Knisely (1990), Norberg (1993)], most of the results are applicable to higher Reynolds number [$\geqslant 400$ for Knisely (1990) and Norberg (1993)], and their emphasis is not on the mode A and B instabilities. On the other hand, most of the papers that reported on the three-dimensional wake of a square cylinder are not experimental. Robichaux et al. (1999) performed three-dimensional Floquet analysis on the square cylinder wake, and reported on a long-wavelength mode A instability with a wavelength of about 5.2 times the cylinder side-length which first becomes unstable at a Reynolds number of about 161; followed by a short-wavelength mode B instability with a wavelength of about 1.2 times the cylinder side-length which becomes unstable at a Reynolds number of around 190. In addition, they also reported a third intermediate-wavelength sub-harmonic mode (mode S) with a wavelength of about 2.8 times the cylinder side-length. More recently, Blackburn and Lopez (2003b) re-analyzed the wakes of circular and square cylinders by Floquet analysis. They reported that the intermediate-wavelength mode for the square cylinder should be quasi-periodic (mode QP), just like the case of a circular cylinder; and the Floquet multiplier used should be a complex conjugate, not just a real number as used by Robichaux et al. (1999). DNS investigation of the square cylinder wake at moderate Reynolds numbers ($Re = 150$–500) was carried out by Sohankar et al. (1999), their simulations indicated a transition from 2-D to 3-D shedding flow at Re somewhere between 150 and 200. Both spanwise instability modes A and B were present in the wake transitional process. Via numerical simulation about the wake transition of square cylinder, Saha et al. (2003) reported that the critical Reynolds numbers for mode A and mode B instabilities are 175 and 250, respectively. In Blackburn et al. (2005), by making use of the half-period-flip

map in Floquet stability analysis, they showed that there are exactly three codimension-one bifurcations from two- to three-dimensional flow. Two of them were found to be synchronous (modes A and B reported by most other researchers), while the third is quasi-periodic (the intermediate wave length mode reported by both Barkley and Henderson, 1996 and Robichaux et al., 1999). The only recent experimental work on square cylinder wake instabilities known to the authors is the work of Luo et al. (2003). They confirmed the existence of mode A and mode B instabilities in the square cylinder wake experimentally. Through flow visualization, they also found that the critical Reynolds numbers for transition to mode A and B instability to be 160 and 200, respectively.

The main objective of the present study is to gain better understanding of the flow around a square cylinder in the low Reynolds number regimes, including the transition processes that take place in the wake.

In the present work, three types of measurements were conducted to address different aspects of the transition processes in the wake of a square cylinder. They are hot-film anemometry, flow visualization and particle image velocimetry (PIV). Among them, hot-film anemometry (see Section 3) was used to identify the critical Reynolds numbers of different instability modes, and the characteristics of each flow regime. At the same time, flow visualization (see Section 4) provides an overall insight into the secondary instabilities, from which the symmetries and structures of different instability modes could be reviewed. Last but not least, by utilizing PIV (see Section 5), quantitative data such as the vorticity and circulation of vortices and wavelength of secondary vortices, etc. were measured, which hopefully will provide some further indications on how the transition processes had happened.

2. Experimental set-up

In the present investigation, two flow facilities were used. One is a vertical water tunnel and the other a horizontal water channel. Due to its ability in executing small changes in flow velocity, the vertical water tunnel was chosen for the investigation of the transition process in a cylinder wake via hot-film measurements. On the other hand, flow visualizations and the PIV measurements were carried out in the horizontal water channel for its bigger test-section (which takes in larger models for the same amount of blockage) and its open top and free surface (which facilitate the insertion of measuring equipments into the flow).

The cross-section of the test-section of the low speed recirculating vertical water tunnel is 200 mm × 200 mm and it has a length of 600 mm. Away from the boundary region the streamwise turbulence intensity varies within 1%. In this tunnel the uncertainty in the Reynolds number is estimated to be about 1–2%, while the uncertainty in the Strouhal number measured is about 1.5–2.5%.

The horizontal water channel is also of the recirculating design. The test-section is 183 cm in length and has a 40 cm (W) by 45 cm (H) cross-section. It was entirely fabricated out of plexiglas, thus allowing easy high-quality flow visualization from almost any angle. Within the flow range used in the current investigation, the turbulence intensity is about 1–2%. The uncertainty in the Reynolds number is about 2–3%. The accuracy of the vorticity measured via the PIV approach was estimated to be about 11.3% and 5.6% for mode A and mode B flow, respectively.

For hot-film measurements in the vertical water tunnel, a polished stainless steel square cylinder with a side-length (D) of 3.15 mm was used. End-plates with different inclination angle were installed at the end of cylinders, either to investigate the effects of end conditions or to maintain parallel shedding. A Dantec hot-film anemometer linked to a CTA system was used to measure the flow field. The data were processed by using a DT translation card, which was installed in a PC. HP-VEE software package was used for acquiring and processing data.

A hollow aluminium square cylinder with a side length of 7.8 mm was used as the experimental model for the flow visualization of streamwise vortices in the horizontal water channel. For the ejection of dye, a spanwise slot with a length of about 250 mm was made on the upper surface of the cylinder. End-plates that were inclined inward (toe-in) at 16–18° were installed in order to maintain parallel vortex shedding. Dye was released slowly through the slot and washed downstream. Ordinary dye visualization and laser-induced-fluorescence dye visualization were used to demonstrate the vortex structure in the X–Z plane and Y–Z plane, respectively. The coordinate system used in the current investigation is shown in Fig. 1, the origin is at the mid-point of the square cylinder rear face.

Flow images from the experiments were recorded by a Panasonic AG-7355 video cassette recorder through a Sony CCD-IRIS color video camera (Model: DXC-107P). The flow visualization images were later extracted from the video recording by using a video capture programmer (Matrox Rainbow Runner).

For PIV measurements in the horizontal water channel, several square cylinder models and a circular cylinder model were used. For the measurements of secondary vortices in the mode A regime, a square cylinder with a side length of 4.73 mm was used. In the mode B regime, a square cylinder with a side length of 9.5 mm was used. The circular cylinder used had a diameter of 9.5 mm. For each case, end-plates with optimal inclination angles were installed to maintain

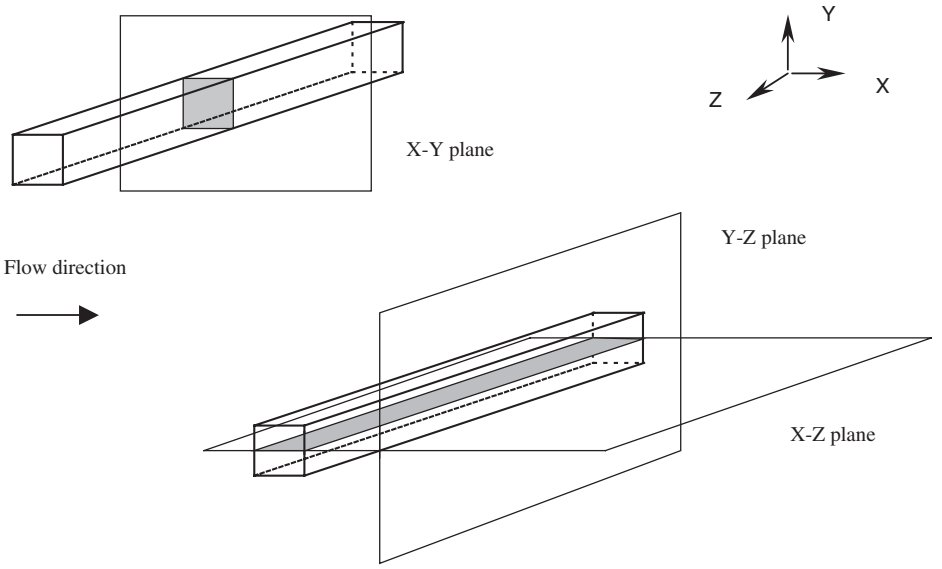

Fig. 1. Principal coordinates and planes of the laser sheets used in flow visualization and PIV measurements. The origin is at the mid-point of the rear side of the square cylinder.

parallel shedding. In the current investigation, a Dantec PIV2100 processor system with a Continuum 200 mJ Nd:YaG laser system which is capable of producing 2×200 mJ laser pulses at 10 Hz were used. Optimage particles with diameter of 30 and 60 μm and specific gravity of 1.2 were used as seeding tracers. Scattered light from the particles was captured by a Kodak ES 1.0 Megapixel 8-bit Digital CCD Camera with a CCD array size of 1016 pixels × 1008 pixels. The camera was placed perpendicularly to the plane of the laser sheet and the recorded particle image pairs were transferred to a workstation for post-processing. The time interval between laser pulses and the time interval between recordings were set according to different experimental conditions. For post-processing, the Dantec FlowManager software was used to derive the velocity and vorticity fields.

For all the work reported in this paper, the upstream side of the square cylinder is always normal to the freestream (angle of attack is always equal to zero degree). The cylinder aspect ratio is defined as the ratio between the distance between the leading edges of the end plates and the cylinder side length D. Further details of the experimental set-up can be found in Tong (2003).

Table 1 provides a summary of the experimental parameters of the three present experiments.

3. The determination of flow regimes and the velocity characteristics

3.1. The effects of cylinder end conditions and aspect ratio

Strictly speaking, with the exception of very low Reynolds numbers, all real flows are three-dimensional. Different end conditions and aspect ratio (L/D_0), where L is the length and D_0 is the diameter, have been found to have strong influences on the wake of a circular cylinder. The methods to modify cylinder end conditions include: use of angled end plates (Williamson, 1988a), use of coaxial end cylinders (Eisenlohr and Eckelmann, 1989), use of novel control cylinders which are orthogonal to the test cylinder (Hammache and Gharib, 1989, 1991), and use of suction tubes from downstream (Miller and Williamson, 1994). Recently, Luo et al. (2001) also demonstrated that the use of inclined end-plates could promote and maintain parallel vortex shedding in both circular and square cylinder flows. In the present investigation the inclined end-plate method was chosen due to its simplicity and flexibility.

The parameter used to reflect the effects of end conditions and aspect ratio is the Strouhal number (St), which is defined as

$$\mathrm{St} = \frac{fD}{U_0}, \tag{1}$$

Table 1
Summary of experimental parameters

Experimental methods	Side length of square cylinder D, material used	Diameter of end plates, D_e	Aspect ratio[a]	Size of test-section	End-plate inclination angle (degrees)
Hot film	3.15 mm, polished stainless steel	70 mm	59, 57, 54, 52, 51	$200 \times 200 \times 600$ mm	0, 7, 14[b], 18, 22
Flow visualization	7.8 mm, hollow aluminum square cylinder	120 mm	41	$400 \times 450 \times 1830$ mm	16–18[c]
PIV					
1) von Karman vortices	9.5 mm, aluminum	120 mm	34	$400 \times 450 \times 1830$ mm for both cylinders	16–18
	9.5 mm diameter circular cylinder	120 mm	33.68		16
2) Secondary vortices (mode A)	4.73 mm, stainless steel	80 mm	72	$400 \times 450 \times 1830$ mm	16–18
3) Secondary vortices (mode B)	9.5 mm, aluminum	120 mm	34	$400 \times 450 \times 1830$ mm	16–18

[a]In the present paper, aspect ratio is defined as distance between the leading edges of the end-plates over side length D of the square cylinder (or diameter of the circular cylinder).

[b]Other than the study of end effects, in which end-plate inclinations of 0°, 7°, 14°, 18° and 22° were investigated, in other measurements the optimum end-plate inclination of 14° was used.

[c]For the study of end effects, besides the optimum end-plate inclination of 16°–18°, parallel end-plates (0°) were also used.

where f is the predominant vortex shedding frequency, D is the side length of the square cylinder, and U_0 is the free stream velocity. As suggested by Williamson (1988a) for circular cylinder wakes, parallel vortex shedding has the largest corresponding St magnitude, and an approximate (cosine law) relationship relates the oblique shedding and parallel shedding frequencies in the laminar shedding regime. The cosine law is

$$\mathrm{St}_0 = \frac{\mathrm{St}_\theta}{\cos\theta}, \tag{2}$$

where θ is the oblique shedding angle, and St_θ and St_0 are the oblique and parallel vortex shedding Strouhal number, respectively. The optimum end-plate inclination angle can be found by measuring the variation of Strouhal numbers with end-plate inclination angle.

In the present experiment a hot film was positioned outside the separated shear layers in the near-wake region ($Y/D \approx 1.5$ and $X/D \approx 6$), and very close to the mid-span ($Z/D = 0$) of the cylinder. Circular end-plates with diameter (D_e) of 70 mm and inclined at 14° (toe-in) were installed to promote and maintain parallel shedding. The corresponding D_e/D ratio is therefore approximately 22.22. They were placed 170 mm apart on the cylinder, resulting in an effective aspect ratio (L/D) of 54. For the investigation on end-plate inclination, five different pairs of end-plates with equal diameter were used. When installed, they are inclined inward (toe-in) at angles of 0°, 7°, 14°, 18° and 22° to the free stream. With the distance between the (inward inclined) leading edges of the end-plates as the effective span, the effective aspect ratio of the cylinder varies from 51 (end plates inclined at 22°) to 59 (parallel end plates).

In the present investigation, the predominant vortex shedding frequency is determined from the mean of six wake velocity spectra. The St–Re relations for the wake of a square cylinder with different end-plate inclination angles are shown in Fig. 2. The effects of end plates inclination are clearly demonstrated. In both the laminar ($\mathrm{Re} < 160$) and transitional ($\mathrm{Re} > 160$) flow regimes, the magnitude of the Strouhal number increases with end-plate inclination, but the rate of increase reduces at large end-plate inclination. There is only a very small difference between the curves for 14° and 18° end-plate inclination. When the end-plate inclination was further increased to 22°, the St data effectively coincide with those at end-plate inclination of 14° and 18° in the Re range of 70–110. At $\mathrm{Re} > 110$, the flow becomes unstable, presumably due to stalled aerofoil-like flow separation at the end-plate leading edges. Accordingly, 14° is thought to be the most optimum end-plate inclination angle in hot-film measurements. However, it should be emphasized that the optimum end-plate inclination is likely to be dependent on experimental set-up/conditions (which may include the cylinder aspect ratio), and 14° is not a universal value. In fact, in the flow visualization and PIV work reported in the later part of this paper, the most optimum end-plate inclination angle was found to be around 16–18°.

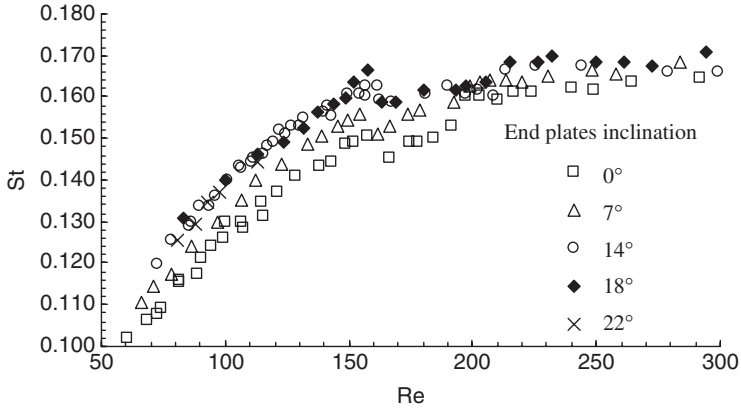

Fig. 2. The effects of end-plate inclination on Strouhal number.

In four of the above-mentioned St–Re curves (except the 22° case), there are two discontinuities that take place at different Reynolds numbers. These discontinuities mark the inception of different instability modes, namely mode A and mode B instabilities. For the cylinder with 14° inclined end-plates, mode A appears at about $Re_c = 160$ (Re_c here refers to a critical Reynolds number at which some flow instability emerges). Above Re of about 204–210, only mode B can be detected (no large-scale low-frequency disturbances detected). For the cylinders with 0° and 7° inclined end-plates, the two critical Reynolds numbers are a little lower than those of the 14° end-plate cylinder (near 156 and slightly lower than 204, respectively). This is likely to be a consequence of the oblique shedding when the end-plate inclinations are smaller than 14°. The presence of the two discontinuities (with the first one at $Re_c \approx 160$ showing hysteretic behaviour) agrees with the situation in the circular cylinder St–Re curve, but the magnitudes of the critical Reynolds numbers are different. However, the present finding contradicts an earlier report (Luo et al., 2003) where it was reported that discontinuities in the St–Re curve were not captured. The most likely cause of this discrepancy is the use of different flow facilities. Further discussion on the cause of this discrepancy is deferred to the end of Section 3. Among the papers (square cylinder, experimental investigations) in the literature that we are aware of, none of them had obtained the St–Re data at sufficiently small increments in Re to demonstrate the presence of the discontinuities.

Besides the above-discussed, another interesting observation made in the present investigation is that beyond the second critical Reynolds number (transition to mode B instability), the difference among the Strouhal numbers that correspond to different end-plate inclinations becomes smaller when compared to those in the mode A regime and laminar flow regimes (see Fig. 2). This observation suggests that the end-condition effects may have become weaker in the mode B regime.

For aspect ratio effects, the results (all obtained with 14° toe-in end-plates) are shown in Fig. 3. It can be seen that when the aspect ratio is less than 22.2, the magnitude of the Strouhal numbers increases with the cylinder aspect ratio. On the other hand, when the aspect ratio is larger than 22.22, the Strouhal number is almost unchanged. The above suggests the existence of some sort of critical aspect ratio and it is likely to be between 15.9 and 22.2, above which the Strouhal number is independent of (or only weakly dependent on) the cylinder aspect ratio. Based on the results of above investigations, 14° inclined end-plates were used for the rest of hot-film measurements, and the largest possible aspect ratio was always adopted.

3.2. *The transition process in the wake of a square cylinder*

With the installation of the 14° inclined end-plates to induce parallel vortex shedding in the laminar regime, the St–Re relation is obtained and shown in Fig. 4. Two discontinuities were observed in the present St–Re relation. They mark the inception of mode A instabilities and the transfer from mode A to mode B instability. A slight hysteresis (over a Re range of less than 6) is observed at the first discontinuity but not the second one.

From the present results, Re_{c1} was found to be around 160 (determined from increasing Reynolds number) and Re_{c2} was found to be about 204 ± 5. There are very few experimental works addressing the transitional wake of a square cylinder. Among them, Luo et al. (2003) reported that the two critical Reynolds numbers are 160 and 200 (estimated from flow visualization). Although the magnitude of the critical Reynolds number agrees quite well with the present

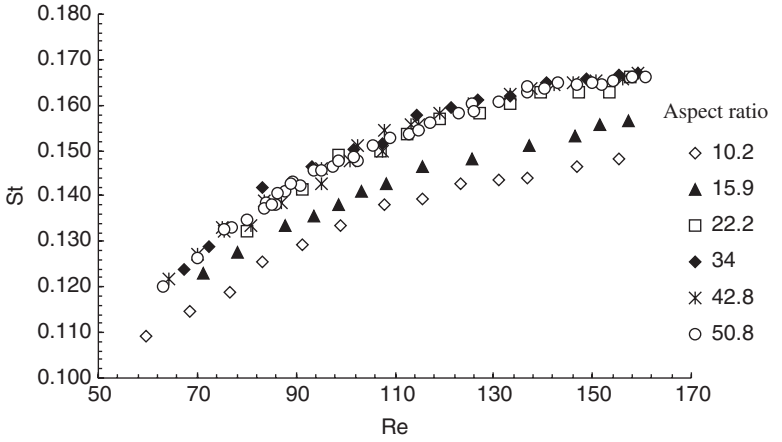

Fig. 3. The effects of cylinder aspect ratio on Strouhal number (with end-plates inclined at 14° toe-in).

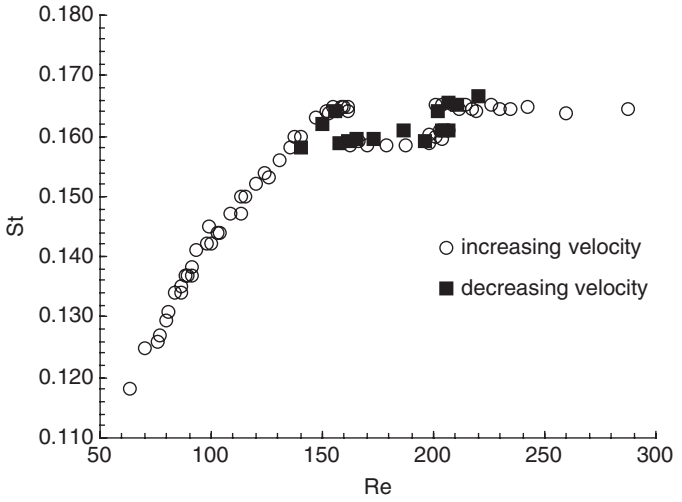

Fig. 4. Strouhal–Reynolds number relationships for flow past a square cylinder (with end-plates inclined at 14° toe-in and effective cylinder aspect ratio of 54).

findings, Luo et al. observed relatively gradual changes in the St–Re curve and reported no discontinuities at the two critical Reynolds numbers. This is different from the present findings, and the discrepancy may arise from the differences in experimental set-up and conditions. The St–Re curve in the present work was obtained from work done in a small vertical water tunnel, where fine speed increment was possible (Section 2). On the other hand, the St–Re curve reported in Luo et al. (2003) was obtained in a wind tunnel, where small and accurate variations in Re was hampered by the resolution of the micromanometer used [a ΔRe (experimental increment in Reynolds number) of ± 4 was mentioned in Luo et al. (2003)]. Apart from experimental research, some analytical and DNS studies also shed light on the transition process of a square cylinder wake. Robichaux et al. (1999) had shown that mode A appears at a Reynolds number of around 161 and mode B appears at a higher Reynolds number of around 190. Sohankar et al. (1999) indicated that the transition from 2-D to 3-D was between $Re = 150$ and 200. Recently, Saha et al. (2003) suggested the inception of mode A instability is at around $Re = 150$–175, while the critical Reynolds number for mode B is about 250 from their DNS investigation. All the above results are in reasonably good agreement with present experimental results. However, it should be pointed out that none of the earlier work reported had obtained St–Re data at sufficiently small increments in Re to demonstrate the presence of discontinuities in the square cylinder St–Re relation, and the present work [which includes the authors' earlier conference paper (Luo et al., 2001)] may well be the first one to do so. For the ease of reference and comparison, all the critical Reynolds number mentioned above are summarized in Table 2.

Table 2
Summary of critical Reynolds numbers reported/found

Researchers	Re_{c1}	Re_{c2}	Methods
Robichaux et al. (1999)	162 ± 12	190 ± 14	Floquet analysis
Norberg (1996)[a]	150		Experimental St–Re measurement (method used not clear)
Sohankar et al. (1999)	2-D to 3-D transition occurs between Re = 150 and 200		DNS
Saha et al. (2003)	150–175	250	DNS
Luo et al. (2003)	160	200	Experiment-flow visualization
Present	160 ± 2	204 ± 5	Experimental St–Re curve measurement (hot film)

[a]Norberg (1996) is unpublished work mentioned in Sohankar et al. (1999).

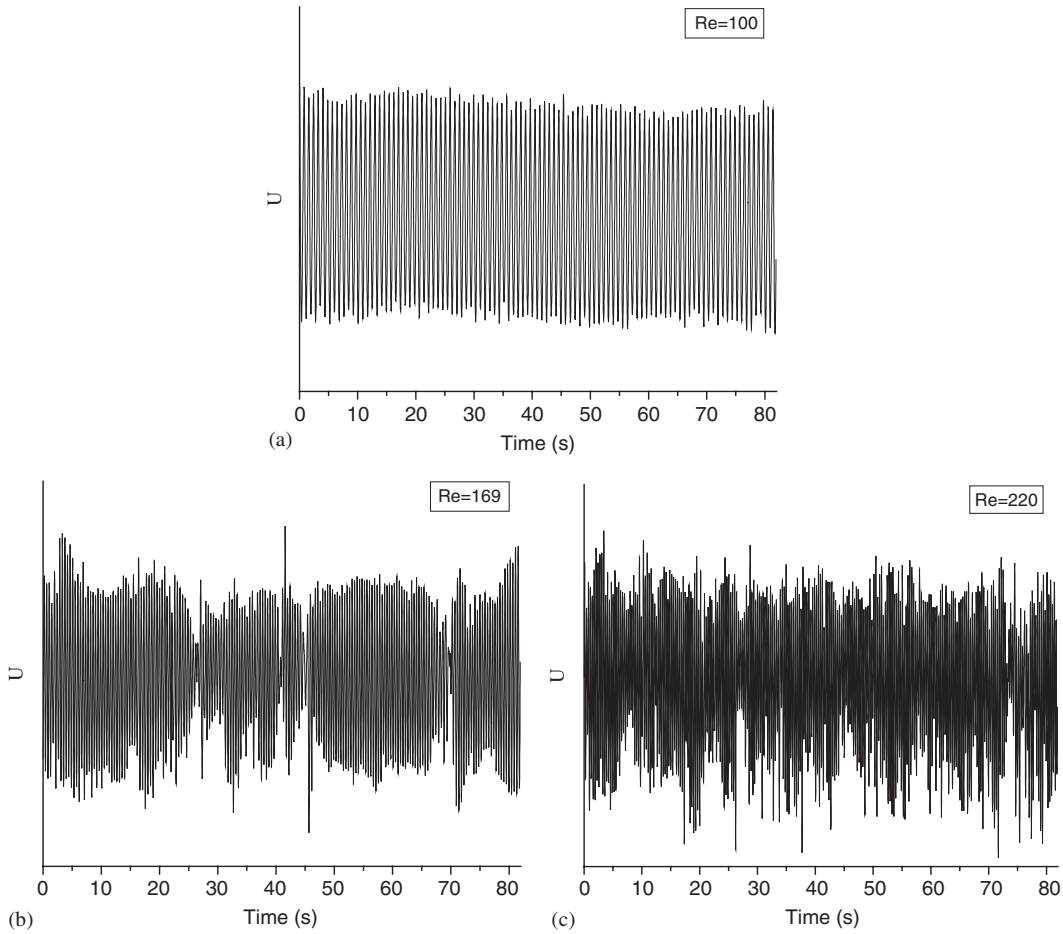

Fig. 5. The time traces of streamwise velocity in a square cylinder wake at different Reynolds numbers.

When the Reynolds number is increased from a fairly low value of about 60, the wake of a square cylinder will undergo laminar, mode A and mode B regimes in sequence until it finally becomes turbulent. Three distinct time traces of the streamwise velocity component corresponding to the three flow regimes in a square cylinder wake at different Reynolds numbers are shown in Fig. 5. In the laminar regime (Re = 100), it can be seen that the variation of streamwise

velocity with time is nearly perfectly periodic. In the mode A instability regime (Re = 169), the regularity in the velocity fluctuation is generally present, but at some instances there is a sudden decrease in velocity magnitude. It is these sudden decreases in velocity magnitude that mark the presence of mode A instability. The sudden decreases in velocity magnitude in the case of circular cylinder wake were referred to as "glitches" by Williamson (1992). Finally, for the case of Re = 220 which was supposed to be in the mode B regime, a more "uniform" disorder in the variation of velocity magnitude is observed. This suggests that the low-frequency disturbances in the mode A region which are reflected as "glitches" have given way to the more "uniform" disorders and eventually evolved into turbulent flow. It was also noted that before the Reynolds number reaches Re_{c1}, some transient transition can already be observed. Such transitions are called "transient" because, although the "glitches" which mark the appearance of mode A can be observed, they appear infrequently and are short-lived.

The transition process of a square cylinder wake is also reflected in the evolution of the wake velocity spectra, shown in Fig. 6. It can be seen that the spectra also display three different patterns which correspond to laminar regime (Re = 150), mode A regime (Re = 162–198), and mode B regime (Re = 216 and 228). In the laminar regime, a sharp peak is present in the spectrum. In the mode A regime, a broader "peak" is seen in the spectrum which suggests that the flow energy was distributed over a wider frequency range. Experimental evidence shows that those "glitches" cause the broadening of the spectral peak, and a drop in Strouhal number. The pattern of the velocity spectra in the mode B regime comes in-between those in the laminar and mode A regimes, with a spectral peak sharpness that also comes in between the two above-mentioned regimes. A double peak spectrum was also observed at Re = 198. Similar double peaked spectra had also been noted in circular cylinder flows. Also like the case of circular cylinder as reported in Williamson (1996a), the twin peaks result from the intermittent swapping between the lower-frequency mode (mode A) and the higher-frequency mode (mode B) at the transitional Reynolds number, and can only be seen in a spectrum that covers data over a sufficiently long period of time.

Before ending the present session, let us return to the difference in St–Re relation between the present work (where two discontinuities were observed) and the results reported in Luo et al. (2003) (where St varies relatively smoothly with Re and with no distinct discontinuities observed). Earlier it was suggested that the possible reason for the hysteresis phenomenon (onset of mode A instability) not to be detected in Luo et al. (2003) is because of the inability of the experimental set-up to capture small increases in Re (ΔRe of ± 4 was quoted). In addition to the above explanation, we also note that Williamson (1996a) had suggested that the effects of vortex dislocation (those that cause the "glitches" in the mode A regime), if present in the mode B transition, can result in the absence of a discontinuity (sudden increase) at Re_{c2} in the St–Re relation. It is also known [again from Williamson (1996a)] that in circular cylinder flows, if vortex

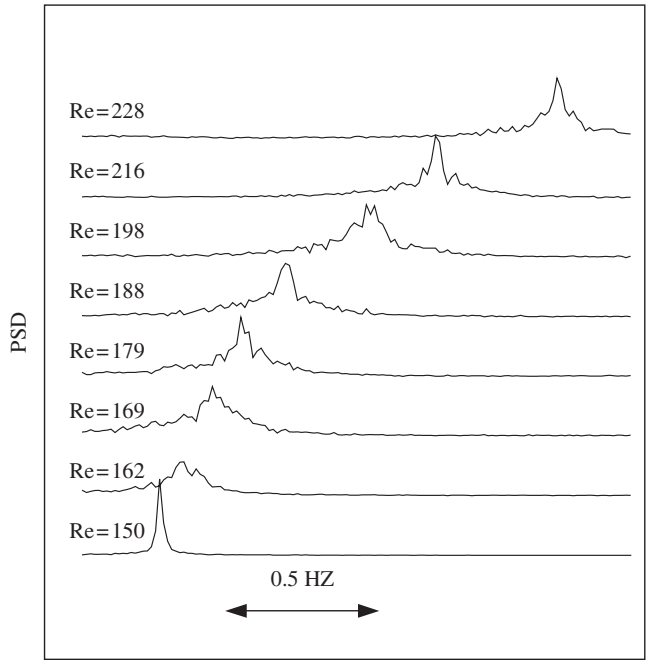

Fig. 6. The evolution of the wake velocity spectra from the laminar to the mode B regime.

dislocation is absent in the mode B transition flow, the transition from mode A to mode B is characterized by a twin peak spectrum comprising of the frequencies associated with mode A and mode B vortex shedding. It appears that in the flow in Luo et al. (2003), vortex dislocation is present in the mode B regime (as evidenced in the velocity–time trace at Re = 223 shown in their Fig. 4). The associated consequences are the absence of a discontinuous jump in St in the mode A to mode B transition, and the absence of a twin-peaked wake velocity spectrum [Fig. 5 of Luo et al. (2003)]. The mode B regime in Luo et al. (2003) is therefore rather like the "B* regime" mentioned in Williamson (1996a) [this is despite the fact that data reported in Luo et al. (2003) were acquired only after sufficient time was given for the flow in the wind tunnel to reach some sort of stable condition]. On the other hand, it appears that vortex dislocation is absent in the mode B flow in the present work (Fig. 5(c)), and the associated consequences are a discontinuous jump in St during the mode A to mode B transition, and the presence of a twin-peaked wake velocity spectrum (Fig. 6, Re = 198); just like the (mode B regime) case of a circular cylinder flow. So it seems that there are differences between the mode B flow in Luo et al. (2003) and the present work. The differences are consistent with the mode B* versus mode B (Williamson, 1996a) situation in circular cylinder flows. However, other than a broad reason like "differences in experimental set-ups", which includes the use of 14° inclined end-plates to reduce the effects of end conditions in the present work [end-plates were also used in Luo et al. (2003) but they were parallel], at present we are not able to offer any further explanation on what causes the differences noted.

4. Evidence from flow visualization

4.1. The existence of mode A and mode B instabilities

With the installation of inclined end-plates (typically 16–18° for the current set-up), parallel vortex shedding was promoted and maintained. As a result, any three-dimensionality due to the cylinder end-effects was reduced to a minimum. The (X–Z plane) spanwise view of vortex shedding can be seen in Fig. 7. Four Reynolds numbers were chosen, with one each in the laminar regime and mode A regime; and two in the mode B regime. A laminar shedding pattern is observed in Fig. 7(a) (Re = 155), and as expected there are no streamwise vortices between the primary vortices. When the Reynolds number was increased to 188, a typical mode A flow pattern can be seen in Fig. 7(b). The primary vortex cores become wavy along the spanwise direction where some streamwise vortices were pulled out from the primary vortices. With the aid of a $5D$ long scale line, it can be seen that the (spanwise) wavelength of the streamwise vortices is around $5D$. When the Reynolds number is increased to 244 which is within the mode B regime, much finer-scale streamwise vortices can be seen. Although it is hard to determine the exact wavelength of the streamwise vortices, it should be around D to $2D$. When the Reynolds number is further increased to 331, the wake still displays the mode B regime characteristics, although the diffusion effects become somewhat stronger. More accurate spanwise wavelength of streamwise vortices can be determined from PIV measurements and will be presented in Section 5.

4.2. The evolution of streamwise vortices

Laser-induced-fluorescent (LIF) dye was used to explore the evolution and symmetries of modes A and B instabilities. With LIF dye, the camera was placed to look upstream from a location downstream of the cylinder, and normal to a (Y–Z plane) planar light sheet that sectioned the near-wake at around $X = 2D$. In this section, the results of an investigation carried out at Re = 175 (mode A regime) and 235 (mode B regime) are discussed.

The evolution of mode A instability can be seen in Fig. 8 which covers approximately half a vortex shedding cycle. In Fig. 8, two pairs of streamwise vortices are visible, and their separation (spanwise wavelength) is about $5D$. In the following description, we focus on the pair of vortices located near the centre of the photos. In Fig. 8(a), the visible streamwise vortices are in the upper side of braid region. The direction of rotation is marked by a green curve. In Fig. 8(b), the core of the lower side primary vortex is visible and is indicated by the arrow. The two upper side streamwise vortices are still visible, but become less clear. The above is quite similar to the description of Brede et al. (1996), in which they referred to the secondary vortices in mode A regime for the case of circular cylinder wake as "tongues". From Fig. 8(b), it can be clearly seen that the core of primary vortex becomes wavy in the spanwise direction. In Fig. 8(c), the core of primary vortex was moving out of the illumination plane while the two secondary vortices from the lower shear layer were emerging. Finally, in Fig. 8(d), the two streamwise vortices at the lower side braid region appeared with sense of rotation opposite to those from the top braid region which appeared half a cycle earlier (Fig. 8(a)). From the above observation, it can be confirmed that the top and bottom row secondary vortices in

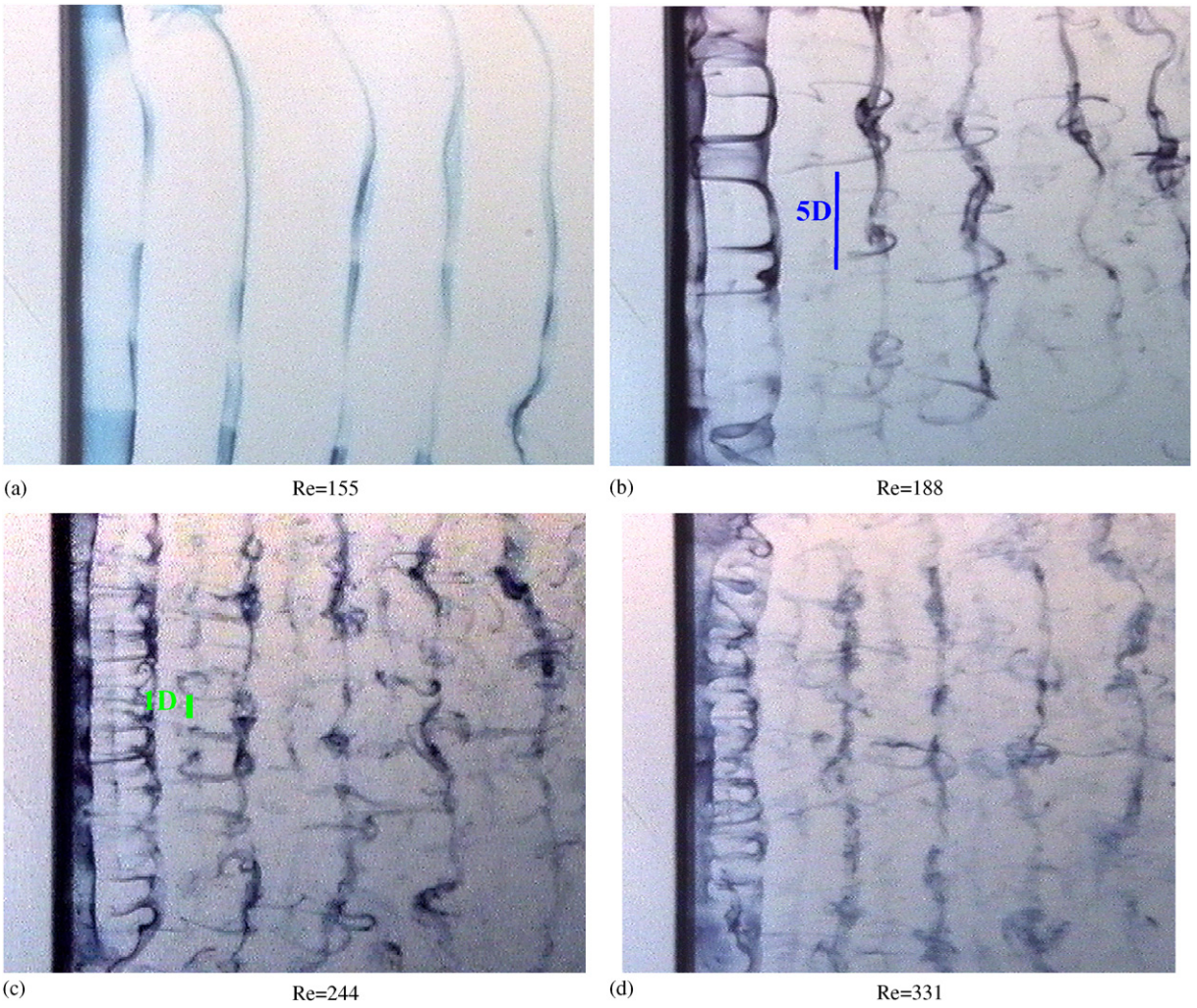

Fig. 7. The wake of a square cylinder (the cylinder is at the extreme left of each picture) at different Re. The cylinder was installed with 16–18° inclined end-plates near it ends (out of picture). Flow is from left to right.

the mode A regime are out-of-phase with each other [referred to as the "symmetric mode" in Blackburn et al. (2005)]. This situation is similar to the flows in the mode A regime reported by Williamson (1996a) (circular cylinder), and Luo et al. (2003) (square cylinder).

Finally, the evolution process of mode B instability is shown in Fig. 9, and like Fig. 8 approximately half a vortex shedding cycle is covered. In Fig. 9(a), mushroom-like vortices at the upper braid region were emerging and the spanwise wavelength is about 1*D*. When compared to the mode A streamwise vortices shown in Fig. 8, it can be seen that the streamwise vortices in the mode B regime are clearer (better defined) than those in the mode A regime. In the next section it will be shown that the vorticity of the secondary vortices in the mode B regime is much higher than those in the mode A regime, which probably explains the observation of better defined streamwise vortices in the mode B regime. In Fig. 9(b), the core of a bottom row primary vortex can be observed, while the secondary vortices were moving downstream rapidly. During this process, the vortex cores of secondary vortices will be projected onto the *X*–*Z* plane. In contrast to the mode A regime secondary vortices, the mode B regime secondary vortices did not cause visible deformation to the primary vortex core, and therefore it is suggested that the formation of mode B streamwise vortices may be somewhat less connected to the primary vortices. In Fig. 9(c), it can be seen quite clearly that it is the secondary vortices from the upper braid region that caused the deformation of the lower braid region. For the case of a circular cylinder wake, this process is referred to as "imprinting" by Williamson (1996a). Comparing Fig. 9(d) with 9(a), it can be seen that the mode B instability is an in-phase mode ["anti-symmetric mode" in Blackburn et al. (2005)] with both

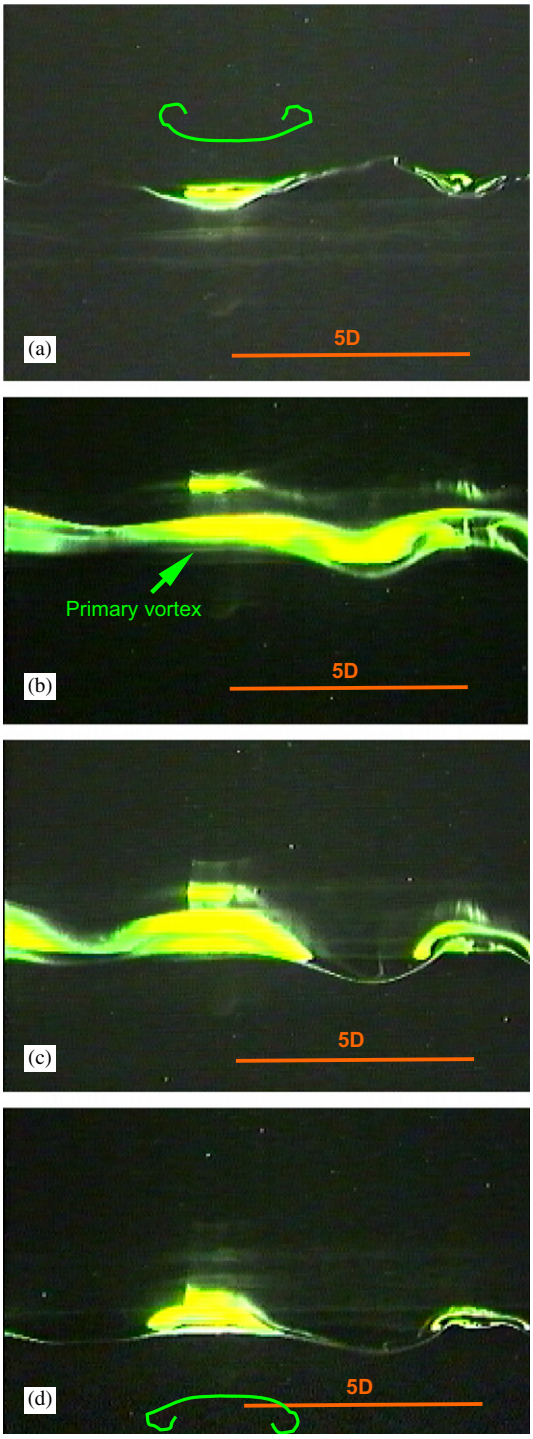

Fig. 8. LIF flow visualization of a cross-flow plane (Y–Z plane) downstream of a square cylinder (at $X \approx 2D$), demonstrating the out-of-phase relation between the top and bottom row streamwise vortices in the mode A regime (Re = 175). Approximately half a cycle of vortex shedding is covered from (a) to (d).

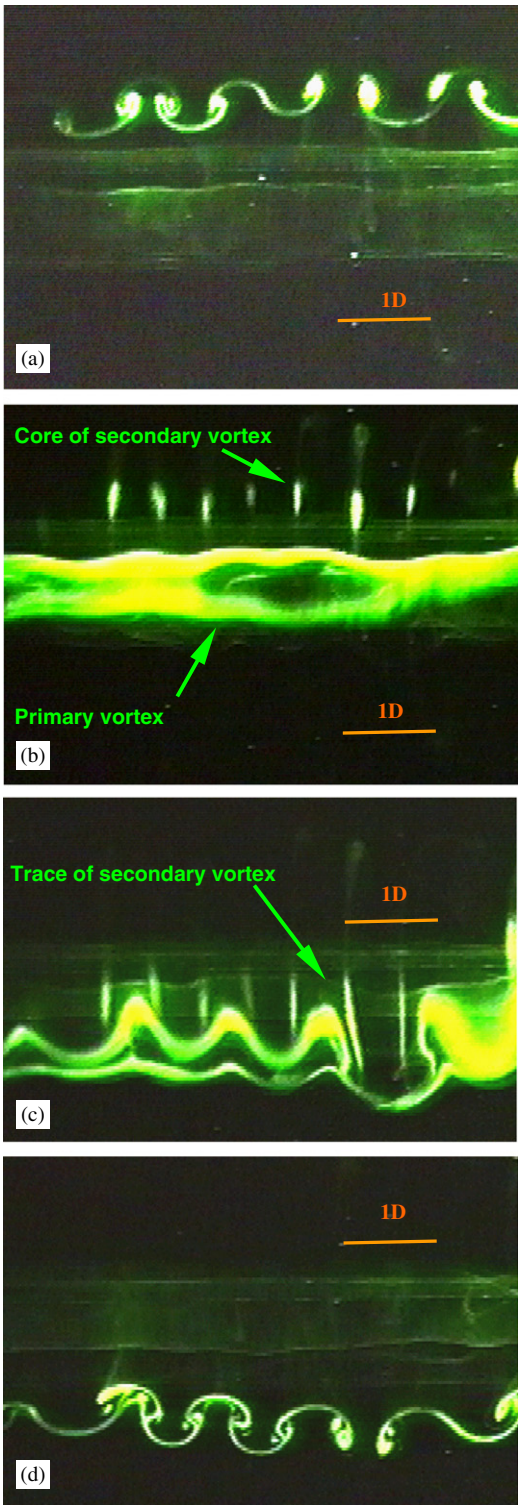

Fig. 9. LIF flow visualization of a cross-flow plane (Y–Z plane) downstream of a square cylinder (at $X \approx 2D$), demonstrating the in-phase relation between the top and bottom streamwise vortices in the mode B regime (Re = 235). Approximately half a cycle of vortex shedding is covered from (a) to (d).

the upper row and lower row streamwise vortices at the same Z (spanwise) location having the same rotation. This is in agreement with Williamson's (1996a) observation for a circular cylinder wake, the Luo et al. (2003) observation for a square cylinder wake, and is opposite to the "out of phase" relation observed in the mode A regime that was reported earlier. Also from the above observation, it can be suggested that there is stronger interaction between braid regions in the mode B regime than in the mode A regime.

5. PIV measurements

5.1. Measurements in the near-wake

In this section, the square cylinder wake at four Reynolds numbers was investigated. The magnitudes of the Reynolds numbers are 138, 176, 243 and 380. The first two Reynolds numbers are within the laminar flow regime and mode A regime, respectively. The last two Reynolds numbers fall within the mode B regime. For the completeness of discussion, we start off with the definition of vorticity.

The Z-component of the vorticity (dimensional) is defined as

$$\omega_Z = \frac{\partial V}{\partial X} - \frac{\partial U}{\partial Y}, \tag{3}$$

where U and V are the components of the velocity in the X and Y direction, respectively. In this paper, the vorticity is calculated by using a second-order central difference scheme, and is then nondimensionalized (to become ζ_z) by the side length of the cylinder (D) and the free-stream velocity U_0:

$$\zeta_Z = \frac{\omega_Z}{U_0/D}. \tag{4}$$

Through studying the laser-induced-fluorescent (LIF) dye visualization reported in Section 4.2, it was noted that a strong interaction exists between the top and bottom streamwsie vortices in the mode B regime, but the corresponding interaction was rather weak in the mode A regime. It is hoped that the quantitative measurement of cross-flow velocity will lead to a better understanding of a square cylinder wake.

To aid discussion below, we wish to introduce two new terms. In the following, we use V_i to represent influencing velocity and V_p to represent penetrating velocity. In fact, both V_i and V_p are (Y-component) cross-flow velocities in the wake region but take place at different times in a shedding cycle. At an arbitrary point above the wake centreline (i.e., in the positive Y region), when V is upward (positive), this upward flow can be interpreted as the positive Y region being affected by the penetration effect of the bottom vortex row. Therefore, the wake cross-flow velocity at this instant and location is designated as a penetrating velocity (V_p). On the other hand, if at the same location V is downwards (negative), it means that the fluid in the positive Y region is getting ready to influence the fluid in the negative Y region. Thus the cross-flow velocity at this moment/location is referred to as an influencing velocity (V_i). In short, in the region above the wake centerline ($Y>0$), the cross-flow velocity V is a V_p if $V\times Y>0$, and a V_i if $V\times Y<0$. At points below the centreline ($Y<0$), the definitions of V_p and V_i are the same. On the wake centreline ($Y=0$), a positive V can be regarded as either a V_p or a V_i, depending on whether we are referring to the top half or bottom half of the wake, respectively. Similar interpretation applies to a negative V on the wake centreline.

In Fig. 10(a), the variation of $V_{i\max}$ (maximum value of V_i (at $X=2D$ and different Y/D)) with Reynolds number is plotted. The $V_{i\max}$ data at $Y=0$ peak at around Re = 243, which is within the mode B regime. At other values of (Y/D), $V_{i\max}$ is either relatively constant or shows a slight increasing trend with Re.

A more interesting observation is made when the variation of $V_{p\max}$ is plotted against Re at $X=2D$ and various Y/D (Fig. 10(b)). The location $X=2D$ is chosen because it is close to the length of the mean wake recirculation bubble (X_r), which is roughly the location the von Karman vortices roll up and cross the wake centreline for the first time. It is believed that V_p at this point can reflect the extent of interaction between vortices more accurately. In Fig. 10(b), at $Y=0$, $V_{p\max}$ peaks at a magnitude of 0.85 at Re = 243 (mode B), and is generally larger in magnitude in the mode B regime. This indicates that at this X-location the interaction between the top and bottom rows of vortices becomes stronger in the mode B regime. More significantly, at $Y=0.5$D, $V_{p\max}$ almost doubles its magnitude when the Reynolds number increases from 176 (mode A) to 243 (mode B), which implies that the penetrating effect at Re = 243 is much stronger than that at Re = 138 and 176. At Re = 380, the magnitude of $V_{p\max}$ is still approximately 1.5 times larger than at Re = 138 and 176. This trend continues so till approximately $Y=2D$.

From the above discussions, it can be seen that, by quantitatively comparing $V_{p\max}$, the difference among different flow regimes becomes clearer. In the mode B regime, vortices are more exposed to the effects from the opposite sign

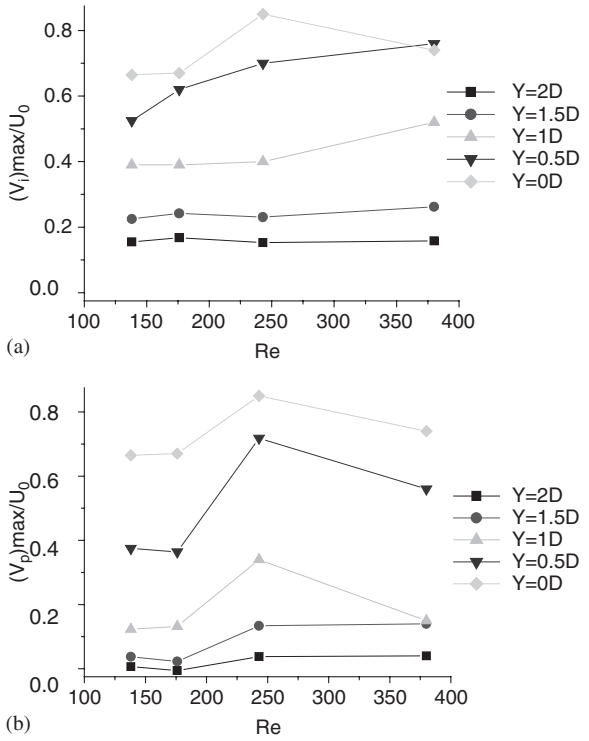

Fig. 10. The maximum "influencing" and "penetrating" cross-flow velocity measured at $X = 2D$ as a function of Reynolds number. (a) Maximum "influencing" cross-flow velocity. (b) Maximum "penetrating" cross flow-velocity.

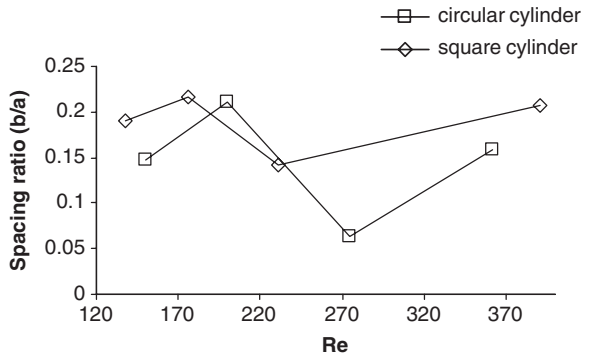

Fig. 11. The variations of spacing ratios (b/a) with Reynolds number.

vortices. This helps to explain why the "imprinting" process proposed by Williamson (1996a) is only significant in the mode B regime, which subsequently results in the "in-phase" relation between the top and bottom rows of streamwise vortices in the mode B regime reported in Section 4.2.

Besides the measurements of cross-flow velocity, the spacing ratio of the von Karman vortex street can also provide some useful information about the difference in various flow regimes. The variations of spacing ratios (b/a) with Reynolds number are plotted in Fig. 11, in which both the measurements of square cylinder and circular cylinder (authors' own data) are presented. In this paper, a represents the spacing between consecutive vortices in the same row, and b is the distance between vortex rows. It should be noted that b generally increases with X. Both a and b were estimated from vorticity contours (PIV results), and represent average values estimated from about 30 to 40 sets of data each.

By examining Fig. 11, it is clear that for both the square and circular cylinders, b/a peaks in the mode A regime. Since in the Re range investigated, a only varies within a narrow range (about 4 to 4.5 times the side length (square cylinder) or diameter (circular cylinder) of the cylinder), the variation in b/a essentially reflects the variation in b. The above therefore suggests that for both square and circular cylinders, the lateral (cross-flow) vortex spacing is largest in the mode A regime, suggesting that the wake cross-flow is likely to be weak in the mode A regime but strong in the mode B regime, consistent with the data shown in Fig. 10(b).

5.2. The study of secondary vortices in the cylinder wake

The objective of the current section is to investigate the structure and the development of secondary vortices in the wake of a square cylinder in the transition regime. Three Reynolds numbers (183, 228 and 377) were investigated in this section. The first Re is in the mode A regime, and the other two are in the mode B regime. Similarly to the previous sections, inclined end-plates (16–18°) were installed at the ends of cylinder to induce parallel vortex shedding. Thus, end-effects, if any, are assumed to be kept to a minimum.

The 3-D secondary vortices can conceptually be described as embedded in the primary vortices. They can therefore be observed both in the X–Z plane and Y–Z plane (see Fig. 1). Due to the limitation of the current PIV experimental set-up, it is only possible to measure the Y-component of the vorticity of the secondary vortex (namely, ω_y) in the X–Z ($Y = 0$) plane. The readers are therefore cautioned to bear in mind that quantitative information of the secondary vortices presented in this paper (e.g., ω_y (vorticity) and Γ_y (circulation)) are only the Y-direction components of the total quantity.

In order to compare the results of the primary and secondary vortices, in this section the Reynolds numbers are chosen to be as close to the values used in the last two sections as possible. Due to the limitations of the horizontal water channel in varying the flow velocity in small steps, most of the time it was not possible to obtain Reynolds numbers identical to those obtained in the vertical water tunnel. Fig. 12 shows the streamline patterns and vorticity contours of the longitudinal (streamwise) vortices in the X–Z plane at $Y = 0$. In all the figures, the velocity vectors were obtained in a frame of reference moving at 60% of the free stream velocity (U_0). There are some common features in these figures: longitudinal vortices are arranged along a line that is approximately parallel to the axis of the cylinder; and the sign of vortices alternates along the spanwise direction. However, there are also differences between modes A and B, with "type of symmetry" being the most noticeable. Secondary vortices in the mode A regime (at a certain constant Z/D) are in a staggered arrangement along the X-direction, that is the vortices will change the sense of rotation every half a shedding cycle which is also referred to as odd reflection-translation symmetry (odd RT symmetry in short) by Robichaux et al. (1999). In a X–Z plane, the above will be reflected as vortices along the X-direction (at a certain fixed Z value) exhibiting the same direction of rotation. This can be seen in Fig. 12(a). On the other hand, streamwise vortices in the mode B regime have an in-line arrangement (the sense of rotation (at a certain constant Z/D) remains the same along the X-direction), which is an even RT symmetry. The above should be reflected as vortices along the X-direction (at a certain fixed Z value) exhibiting alternate direction of rotation. Unfortunately, this cannot be seen clearly in Fig. 12(b) because of the smaller extent of the flow field measured, which results from the much smaller spanwise wavelength in the mode B regime as compared to the mode A regime.

Also, at a certain constant X-coordinate and along the Z-direction, the spacing between the vorticity peaks is generally constant. This suggests that there is a representative wavelength (λ_z) for each mode. It can be seen that the spanwise wavelength for mode A is around $5D$ (Fig. 12(a)) while for mode B it is about $1D$ (Fig. 12(b)). Also, in the mode A regime, the centres in the instantaneous streamline plot are not very obvious and this is partially due to the relatively low magnitude of the vorticity. On the other hand, in the mode B regime centres can be seen clearly which suggests that the vorticity of vortices is quite large and the flow around those points are experiencing intensive straining effect and spinning in direction opposite to the adjacent flow/vortices. Quantitative data will be shown later in this section. The above observations have been verified or supported qualitatively by flow visualization (see Section 4, particularly in Figs. 8 and 9), and are consistent with the PIV measurements for the case of circular cylinder (Brede et al., 1996; Wu et al., 1994).

In order to study the relations between the primary and secondary vortices, the peak value of their vorticity and their circulations were measured. The Y-component of the secondary vortex vorticity (ω_y) and circulation (K_y) are both nondimensionalized by D and U_0 into $\zeta_y(= \omega_y/(U_0/D))$ and $\Gamma_y(= K_y/(\pi D U_0))$, respectively. For each case, about 40 sets of data were averaged to obtain the representative value of peak-vorticity and its corresponding circulation.

The above data are tabulated in Table 3 and plotted in Fig. 13. When compared to the data of the primary vortices (ζ_z and Γ_z), the secondary vortices data (in particular the vorticity data ζ_y) change dramatically with variation in the

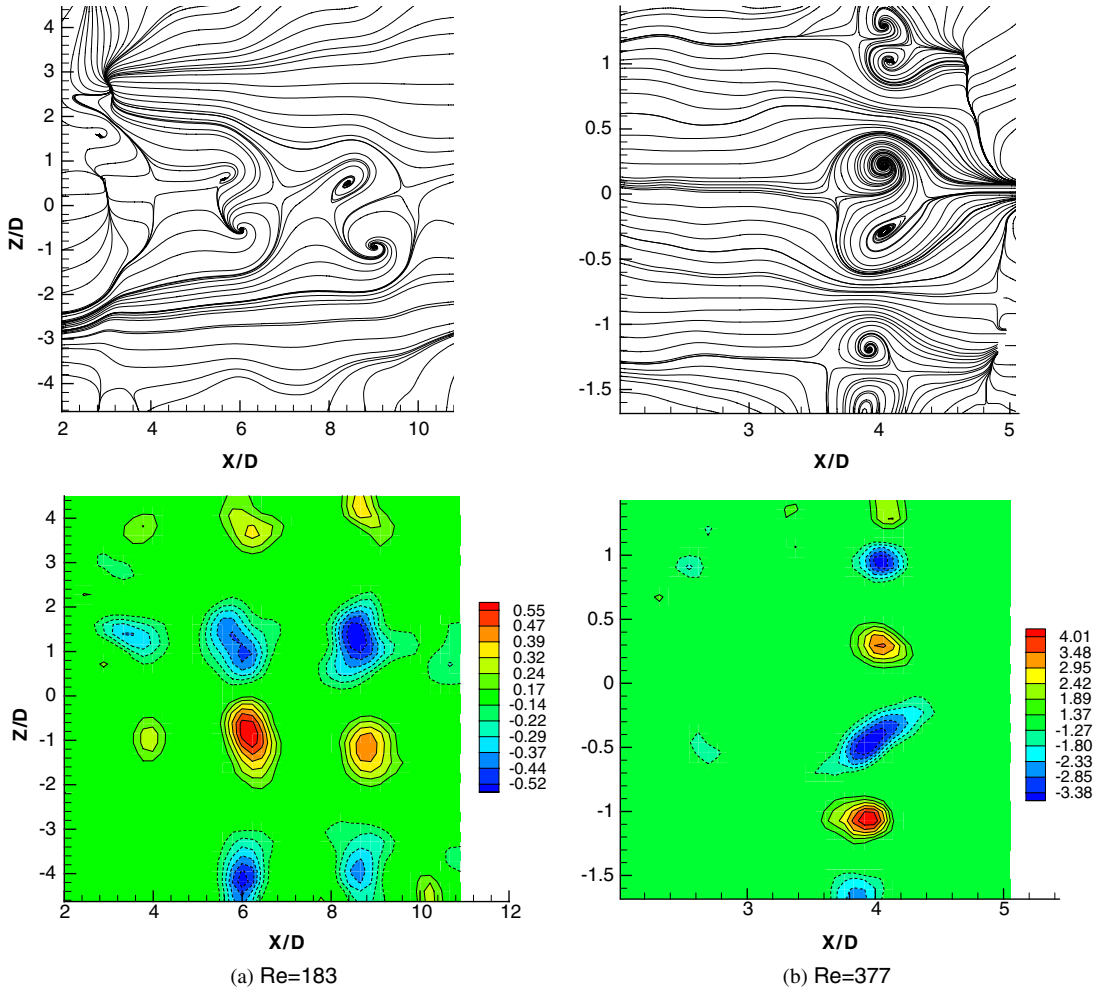

Fig. 12. Instantaneous streamline (top) and vorticity contour (bottom) of longitudinal vortices in the X–Z plane at $Y = 0$.

Table 3
The peak values of vorticity and circulations for primary and secondary vortices

Regime	Primary vortices			Secondary vortices		
	Re	ζ_z	Γ_z	Re	ζ_y	Γ_y
Laminar	138	1.80	1.05			
Mode A	176	1.87	1.17	183	0.62	0.28
Mode B_1	231	2.39	1.09	228	2.68	0.12
Mode B_2	391	2.30	0.94	377	4.13	0.17

Reynolds number. In the mode A regime, ζ_y is considerably smaller (about 1/3) than ζ_z., and the corresponding Γ_y is only about $\Gamma_z/4$. In the mode B regime, ζ_y becomes much larger (larger than ζ_z) and increases with Reynolds numbers. At Re = 380, ζ_y is about 1.8 times the magnitude of ζ_z. At the same time, although the magnitude of ζ_y in the mode B regime is much larger than its counterpart in the mode A regime (four to six times), the corresponding Γ_y is smaller and is only about half of the magnitude of Γ_y in the mode A regime. It can therefore be deduced that the secondary vortices in the mode A regime is larger in size but smaller in vorticity when compared to those in the mode B regime. The above

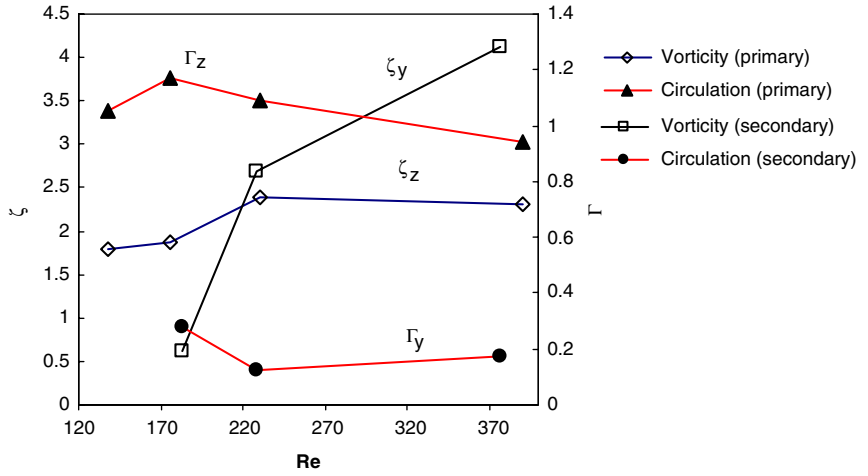

Fig. 13. The comparison of vorticity and circulation between primary vortices and streamwise vortices.

Table 4
Comparisons between primary vortices and secondary vortices for both square and circular cylinders

Re	ζ_y/ζ_z		$\zeta_{y(\text{mode B})}/\zeta_{y(\text{mode A})}$		Γ_y/Γ_z		$\Gamma_{y(\text{mode B})}/\Gamma_{y(\text{mode A})}$	
	Present (square cylinder)	Literature (circular cylinder)	Present (square cylinder)	Literature (circular cylinder)	Present (square cylinder)	Literature (circular cylinder)	Present (square cylinder)	Literature (circular cylinder)
183	0.32	1.62(Re = 525)			0.24	0.11(Re = 525)		0.53[a]
228	1.14	Wu et al. (1994)	4.32(Re = 228/Re = 183)		0.11	Wu et al. (1994)	0.43(Re = 228/Re = 183)	Brede et al. (1996)
377	1.79		6.67(Re = 337/Re = 183)		0.17		0.61(Re = 337/Re = 183)	

[a]The value is $\Gamma_{x(\text{mode B})}/\Gamma_{x(\text{mode A})}$.

results are consistent with those for the circular cylinder wake: Brede et al. (1996) found that the circulation of mode A vortices is twice that of the mode B ($\Gamma_x = 0.3$ at $160 < \text{Re} < 240$ and $\Gamma_x = 0.16$ at $\text{Re} > 240$); while Wu et al. (1994) observed that Γ_y/Γ_z is about 0.11 at Re = 525.

A summary of the present data (square cylinder) and some available data of circular cylinder wake are tabulated in Table 4. It should be noted that because the primary and secondary vortex data were acquired at close but not identical Reynolds numbers, and because the primary vortex data vary only gradually with Reynolds number, interpolation was used to estimate the magnitude of the primary vortex data at Reynolds numbers that correspond exactly to the secondary vortex data, for the computation of the various ratios given in Table 4.

Another important distinction between mode A and mode B instability is in the spanwise wavelength. In this paper the autocorrelation method [see Tong (2003) for details] had been applied to estimate the spanwise wavelength. The calculation is based on the vorticity field and just like the vorticity/circulation data, 40 sets of data were used to obtain a typical λ_z-value. This method of determining spanwise wavelength (λ_z) is more accurate than the magnified pictures method used by many others.

The autocorrelation results for the transition wake of the square cylinder, together with other results from different sources are summarized in Table 5. It can be seen that there is good agreement between present finding and related results obtained by Robichaux et al. (1999) using Floquet analysis and by Luo et al. (2003) using flow visualization. Also from the present investigations, the spanwise wavelength in the mode B regime tends to decrease with an increase in Reynolds number. This is consistent with the observation of Wu et al. (1994) for the circular cylinder wake.

Table 5
Spanwise wavelength of circular cylinder and square cylinder, as multiples of D_0 (diameter) and D (side length), respectively

		Mode A	Mode B_1	
Literature	Circular cylinder	3.96[1]	0.82[1]	
		4.5[2]	1[2]	
		4.01[4]	0.9–0.8[3] (decreases with increase in Re)	
	Square cylinder	5.22[5]	1.2[5]	
		2–5[6]	1[6]	
		3[7]	1.2–1.4[7]	
		5.2[8]	1.2[8]	
Current	Square cylinder	5.1 ± 0.1 (Re = 183)	1.3 ± 0.1 (Re = 228)	1.1 ± 0.1 (Re = 377)

Sources of data: (1) Barkley and Henderson (1996), Floquet analysis. (2) Brede et al. (1996), PIV. (3) Wu et al. (1994), flow visualization and digital imaging analysis. (4) Williamson (1996a), flow visualization. (5) Robichaux et al. (1999), Floquet analysis. (6) Sohankar et al. (1999), DNS. (7) Saha et al. (2003), DNS. (8) Luo et al. (2003), flow visualization.

6. Modes A and B vortex shedding

Some suggested causes of modes A and B instability reported in the literature had been discussed in Section 1 of this paper. By studying the present results, it seems that the elliptic core instability of the primary vortices (Williamson, 1996a) or the centrifugal instability of the braid region (Brede et al., 1996) theory alone may not completely explain the appearance of the mode A instability. Instead, it is likely to be generated from the combination of the stretch effect of the braid region and the deformation of the primary vortices. The evolution of mode A instability could be described in the sequence of scenarios shown in Fig. 14. [Note: The creation of Figs. 14 and 15 has been carried out in reference to similar figures/ideas reported in Williamson (1996a), and Luo et al. (2003).] When the Reynolds number reaches the first critical Reynolds number, there is some small waviness in the primary vortex cores along the spanwise (Z) direction at a certain distance downstream of the cylinder (Fig. 14(a)). This causes the deformation in the vortex sheets around the braid region, and some streamwise vortices become visible (Fig. 14(b)). Due to the feedback mechanism of the vortex sheets, waviness originated in vortex A causes the deformation in the upstream (opposite rotation) vortex B (Figs. 14(c) and (d)). At the same time, the deformed primary vortex cores continue to move downstream. When the process continues, a series of vortex loops could be observed at certain fixed Z-locations (Figs. 14(d) and (e)). Because the effects of the cross-flow (Y-direction) in this flow regime are not strong, the stretching of the vortex sheets is the dominant effect around the braid region and therefore the sense of the secondary vortices is dependent on that of primary vortices and will alternate over every half a shedding cycle.

Considering that the circulation of the secondary vortex peaks at $2D_0$ downstream of the cylinder (for the case of circular cylinder), mode B instability is more likely to be connected with the shear layers that are separated from the cylinder. Also, because the primary vortex cores become relatively isolated (less connections between cores by the braid region), the stretching effect of vortex sheets gives way to the interaction between different vortex rows which is caused by the strong cross-flow, and the feedback mechanism which occurs in the mode A regime to sustain the formation of vortex loops becomes less important. As corroborated by the results of flow visualization (see Fig. 9), the "imprint" process described in Williamson (1996a) is the reason why in the mode B regime the secondary vortices have in-phase symmetry. That is, at a certain Z-coordinate, the rotational direction of secondary vortices will remain the same over the shedding cycles. By combining the above information, the development of the mode B instability could be described as follows: initially, the disturbance is generated in the shear layers (see Fig. 15(b)), and secondary vortices are formed in the braid region (the bottom braid region in the illustration in Fig. 15(b)) in the near wake. Due to the strong interaction between vortex rows near the end of the recirculation region ($1.5D$ to $2D$ downstream of the cylinder, depending on Reynolds number), by the "imprinting effects", secondary vortices with the same sign were generated in the next braid region (the top braid region in the illustration in Fig. 15(c)). As a result, the direction of rotation of the secondary vortices in the two braid regions is the same (in-phase) (Fig. 15(d)). The secondary vortices eventually move downstream with the convection effect of primary vortices, and decay in circulation as they do so.

Building upon some of the related literature mentioned in Section 1, further work is needed to review more about the physical mechanisms at work in both mode A and mode B (and indeed also the mode QP) instability regimes.

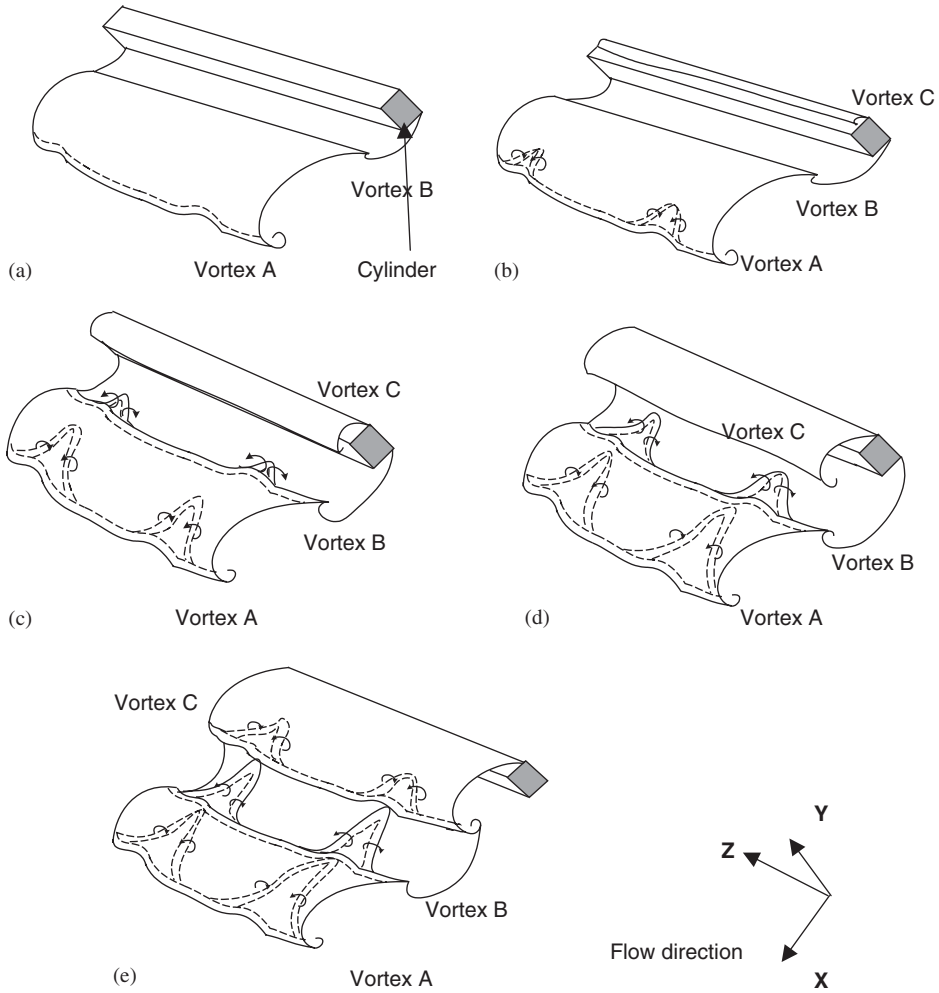

Fig. 14. Sketches of the evolution of secondary vortices in the mode A regime. The free-stream flow is in the X-direction.

7. Conclusions

In the present paper, through both qualitative work (flow visualization) and quantitative work (hot-film anemometry and PIV), the presence of mode A and B instabilities in the wake of a square cylinder are confirmed.

Mode A instability is thought to be caused by a combination of the stretch effect of the braid region and the deformation of the primary vortices. It starts at a Reynolds number of about 160 ± 2, marked by a sudden drop in the Strouhal number in the St–Re relation. Transition to mode A instability is hysteretic. The drop in the Strouhal number is caused by the presence of vortex dislocation, and wake velocity exhibits fairly broad spectral peak. Mode A instability has a spanwise wavelength of about $5.1D$ (at $\mathrm{Re} = 183$), and exhibits an out-of-phase symmetry between the top and bottom row secondary vortices. PIV measurements revealed that in the mode A regime, both the vorticity and circulation of the secondary vortices (ζ_y and Γ_y, respectively) are smaller in magnitude when compared to their primary vortices counterpart (ζ_z and Γ_z, respectively). The vortices in the streamline plot in the X–Z plane are not clear. The cross-flow velocity in the wake is relatively small, consistent with the relatively large lateral vortex spacing in the wake. Finally, based on all the above experimental results, a vortex shedding process in the mode A instability regime is proposed.

Mode B instability, on the other hand, is thought to be caused by an "imprint" process between the two separated shear layers. It is marked by a second discontinuity (sudden increase) in the St–Re relation, and it is not hysteretic. Transition to mode B was noted to take place over $\mathrm{Re} = 204 \pm 5$. The wake velocity exhibits a narrower spectral peak than in mode A, and at certain Reynolds numbers twin spectral peaks were observed. Mode B instability has a spanwise

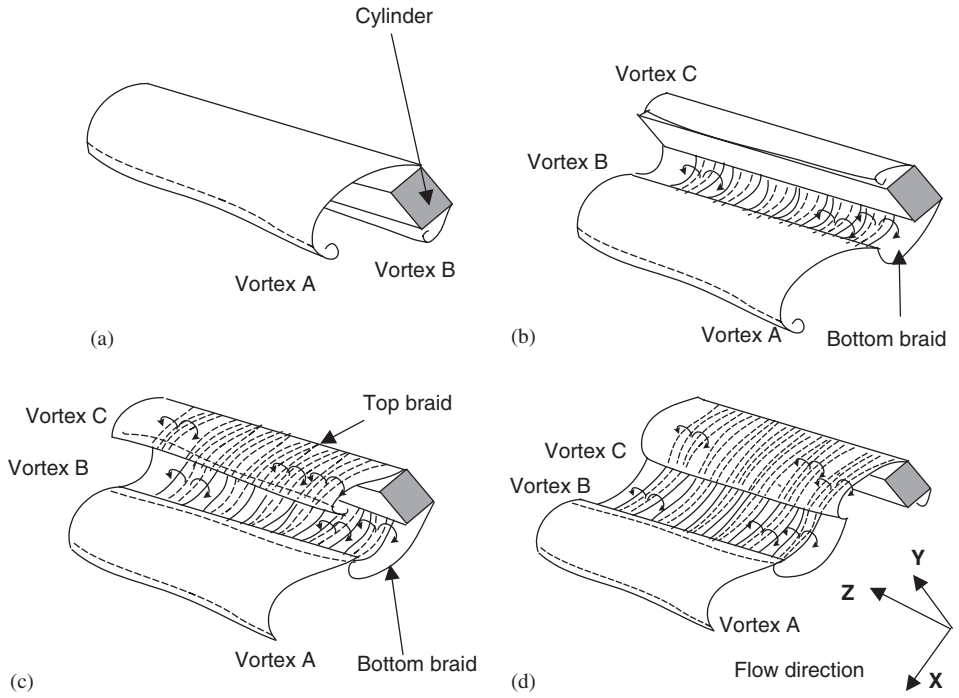

Fig. 15. Sketches of the evolution of secondary vortices in the mode B regime. The free-stream flow is in the X-direction.

wavelength of $1.3(\pm 0.1)D$ and $1.1(+0.1)D$ at $\mathrm{Re} = 228$ and 377, respectively. The "imprint" process suggestion is supported by quantitative data which include a strong cross-flow in the wake region, small lateral vortex spacing ratio and qualitatively by the in-phase relation between the top and bottom row secondary vortices. While the circulation of the secondary vortices is smaller than for their mode A counterpart, the vorticity is significantly larger. This suggests that there are significant straining effects in the flow near the centre of the secondary vortices, and indeed the centre of the secondary vortices can be seen clearly in the X–Z plane streamline plots. Based on the above results, a vortex shedding process in the mode B instability regime is proposed.

Investigation of the effects of end-plate inclination suggests that parallel vortex shedding can be obtained in the end-plates inclination angle range of 14° to 18°. At smaller than ideal end-plate inclination angle, the Strouhal number is smaller in magnitude and the critical Reynolds number is also slightly smaller.

Investigation on the effects of cylinder aspect ratio suggests that there is possibly a critical aspect ratio with a magnitude of between 15.9 and 22.2. Above this critical aspect ratio, variation in the aspect ratio seems to have little influence on the St–Re relation. Below this critical aspect ratio, St increases with cylinder aspect ratio.

References

Barkley, D., Henderson, R.D., 1996. Three dimensional Floquet stability analysis of the wake of circular cylinder. Journal of Fluid Mechanics 322, 215–241.

Bays-Muchmore, B., Ahmed, A., 1993. On streamwise vortices in turbulence wakes of cylinders. Physics of Fluids A 5 (2), 387–392.

Blackburn, H.M., Lopez, J.M., 2003a. The onset of three-dimensional standing and modulated travelling waves in a periodically driven cavity flow. Journal of Fluid Mechanics 497, 289–317.

Blackburn, H.M., Lopez, J.M., 2003b. On three-dimensional quasiperiodic Floquet instabilities of two-dimensional bluff body wakes. Physics of Fluids 15 (8), L57–L60.

Blackburn, H.M., Marques, F., Lopez, J.M., 2005. Symmetry breaking of two-dimensional time-periodic wakes. Journal of Fluid Mechanics 522, 395–411.

Brede, M., Eckelmann, H., Rockwell, D., 1996. On secondary vortices in the cylinder wake. Physics of Fluids A 8 (8), 2117–2124.

Eisenlohr, H., Eckelmann, H., 1989. Vortex splitting and its consequences in the vortex street wake of cylinders at low Reynolds number. Physics of Fluids A 1 (2), 189–192.

Hammache, M., Gharib, M., 1989. A novel method to promote parallel vortex shedding in the wake of circular cylinder. Physics of Fluids A 1 (10), 1611–1614.

Hammache, M., Gharib, M., 1991. An experimental study of the parallel and oblique shedding from circular cylinders. Journal of Fluid Mechanics 232, 567–590.

Henderson, R.D., 1997. Nonlinear dynamics and pattern formation in turbulent wake transition. Journal of Fluid Mechanics 352, 65–112.

Karniadakis, G.E., Triantafyllou, G.S., 1992. Three-dimensional dynamics and transition to turbulence in the wake of bluff objects. Journal of Fluid Mechanics 238, 1–30.

Knisely, C.W., 1990. Strouhal numbers of rectangular cylinders at incidence: a review and new data. Journal of Fluids and Structures 4, 371–393.

Luo, S.C., Khoo, B.C., Tong, X.H., 2001. End effects on cylinder wake transition process. The Fifth Asia-Pacific Conference on Wind Engineering, 21–24 October 2001, Kyoto, Japan, pp. 713–716.

Luo, S.C., Chew, Y.T., Ng, Y.T., 2003. Characteristics of square cylinder wake transition flows. Physics of Fluids 15 (9), 2549–2559.

Miller, G.D., Williamson, C.H.K., 1994. Control of three-dimensional phase dynamics in a cylinder wake. Experiments in Fluids 18, 26–35.

Mittal, R., 1994. A study of flow past elliptic and circular cylinders using direct numerical simulations. Ph.D. Dissertation, University of Illinois at Urbana-Champaign, IL, USA.

Mittal, R., Balachandar, S., 1995a. Vortical structures in bluff body wakes. AIAA 33rd Aerospace Sciences Meeting, January 9–12, Reno, Nevada, USA, Paper 95-0867.

Mittal, R., Balachandar, S., 1995b. Generation of streamwise structures in the bluff body wakes. Physics Review Letters 75, 1300–1303.

Najjar, F.M., Balachandar, S., 1996. Transition dynamics in the wake of a normal flat plate. Bulletin of the American Physical Society 49th Annual Meeting, Division of Fluid Dynamics, Syracuse, NY, 41, 1715.

Najjar, F.M., Balachandar, S., 1998. Low-frequency unsteadiness in the wake of a normal flat plate. Journal of Fluid Mechanics 370, 101–147.

Norberg, C., 1993. Flow around rectangular cylinders: pressure forces and wake frequencies. Journal of Wind Engineering and Industrial Aerodynamics 49, 187–196.

Okajima, A., 1982. Strouhal numbers of rectangular cylinders. Journal of Fluid Mechanics 123, 379–389.

Robichaux, J., Balachandar, S., Vanka, S.P., 1999. Three-dimensional Floquet instability of the wake of square cylinder. Physics of Fluids 11 (3), 560–578.

Saha, A.K., Biswas, G., Muralidhar, K., 2003. Three-dimensional study of flow past a square cylinder at low Reynolds numbers. International Journal of Heat and Fluid Flow 24, 54–66.

Sohankar, A., Norberg, C., Davidson, L., 1999. Simulation of three-dimensional flow around a square cylinder at moderate Reynolds numbers. Physics of Fluids 11 (2), 288–306.

Thompson, M., Hourigan, K., Sheridan, J., 1994. Three-dimensional instabilities in the cylinder wake. International Colloquium on Jets, Wakes and Shear Layers, Melbourne, Australia.

Thompson, M., Hourigan, K., Sheridan, J., 1996. Three-dimensional instabilities in the wake of a circular cylinder. Experimental Thermal and Fluid Science 12, 190–196.

Thompson, M., Leweke, T., Williamson, C.H.K., 2001. The physical mechanism of transition in bluff body wakes. Journal of Fluids and Structures 15, 607–616.

Tong, X. H., 2003. Transition phenomena in the wakes of cylinders. Ph.D. Dissertation, National University of Singapore.

Williamson, C.H.K., 1988a. Defining a universal and continuous Strouhal–Reynolds number relationship for the laminar vortex shedding of a circular cylinder. Physics of Fluids 31, 2742–2745.

Williamson, C.H.K., 1988b. The existence of two stages in the transition to three dimensionality of a cylinder wake. Physics of Fluids 31, 3165–3168.

Williamson, C.H.K., 1992. The natural and forced formation of spot-like 'vortex dislocations' in the transition of a wake. Journal of Fluid Mechanics 243, 393–441.

Williamson, C.H.K., 1996a. Three-dimensional wake transition. Journal of Fluid Mechanics 328, 345–407.

Williamson, C.H.K., 1996b. Vortex dynamics in the cylinder wake. Annual Review of Fluid Mechanics 28, 477–539.

Wu, J., Sheridan, J., Soria, J., Welsh, M.C., 1994. An experimental investigation of streamwise vortices in the wake of a bluff body. Journal of Fluids and Structures 8, 621–635.

Wu, J., Sheridan, J., Hourigan, K., Soria, J., 1996. Shear layer vortices and longitudinal vortices in the near wake of a circular cylinder. Experimental Thermal and Fluid Science 12, 169–174.

Zhang, H., Fey, U., Noack, B.R., Konig, M., Eckelmann, H., 1995. On the transition of the cylinder wake. Physics of Fluids 7, 779–794.